

## Linear dichroism infrared resonance in overdoped, underdoped, and optimally doped cuprate superconductors

A. Mukherjee,<sup>1</sup> J. Seo<sup>1</sup>,<sup>1</sup> M. M. Arik,<sup>1</sup> H. Zhang,<sup>2</sup> C. C. Zhang,<sup>2</sup> T. Kirzhner,<sup>3</sup> D. K. George,<sup>1</sup> A. G. Markelz,<sup>1</sup> N. P. Armitage,<sup>4</sup> G. Koren<sup>1</sup>,<sup>3</sup> J. Y. T. Wei,<sup>2</sup> and J. Cerne<sup>1</sup>

<sup>1</sup>Department of Physics, University at Buffalo, The State University of New York, Buffalo, New York 14260, USA

<sup>2</sup>Department of Physics, University of Toronto, Toronto, ON, M5S1A7, Canada

<sup>3</sup>Department of Physics, Technion, Haifa 32000, Israel

<sup>4</sup>Institute of Quantum Matter, Department of Physics and Astronomy, The Johns Hopkins University, Baltimore, Maryland 21218, USA



(Received 18 July 2019; revised 30 March 2020; accepted 15 July 2020; published 26 August 2020; corrected 25 September 2020)

By measuring the polarization changes in terahertz, infrared, and visible radiation over an extended energy range (3–2330 meV), we observe symmetry breaking in cuprate high-temperature superconductors over wide energy, doping, and temperature ranges. We measure the polarization rotation ( $\text{Re}[\theta_F]$ ) and ellipticity ( $\text{Im}[\theta_F]$ ) of transmitted radiation through thin films as the sample is rotated. We observe a twofold rotational symmetry in  $\theta_F$ , which is associated with linear dichroism (LD) and occurs when electromagnetic radiation polarized along one direction is absorbed more strongly than radiation polarized in the perpendicular direction. Such polarization anisotropies can be generally associated with symmetry breakings. We measure the amplitude of the LD signal and study its temperature, energy, and doping dependence. The LD signal shows a resonant behavior with a peak in the few hundred meV range, which is coincident with the midinfrared optical feature that has been associated with the formation of the pseudogap state. The strongest LD signal is found in underdoped films, although it is also observed in optimally and overdoped samples. The LD signal is consistent with an electronic nematic order which is decoupled from the crystallographic axes as well as novel magnetoelectric effects.

DOI: [10.1103/PhysRevB.102.054520](https://doi.org/10.1103/PhysRevB.102.054520)

Even 30 y after its discovery and hundreds of thousands of publications, high-temperature superconductivity (HTS) in the cuprates remains one of the most enigmatic problems in condensed-matter physics. The rich behavior of cuprates is evident from their complex phase diagram, where different order parameters, each with their own broken symmetries, compete. A key problem is to understand the pseudogap phase. Whether it is just a precursor to superconductivity, a crossover in behavior, or represents a true long-range ordered phase with its own broken symmetry, is unknown.

Although symmetry breaking in cuprate HTS has been theoretically predicted long ago [1,2], it is only recently that terahertz (THz) [3] and near-infrared (NIR) [4–6] polarization-sensitive spectroscopy measurements have discovered the presence of circular and linear polarization anisotropies in HTS cuprates. Polarization anisotropies can in general be associated with the breaking of discrete symmetries. In NIR (800 meV) measurements [4], a small ( $10^{-6}$  rad) polarization rotation in reflection (polar Kerr effect) was measured in  $\text{YBa}_2\text{Cu}_3\text{O}_{6+x}$  (YBCO) in the absence of an external applied magnetic field. In YBCO the polarization signal onsets at a temperature slightly below that of the pseudogap transition temperature  $T^*$ . As a polar Kerr rotation can only arise in a system that breaks time-reversal symmetry [7,8], the polarization anisotropy should be associated with the onset of a time-reversal symmetry-broken phase, possibly one of an unconventional variety [9]. In measurements performed in the THz range (2–6 meV) [3], a large linear dichroism signal, with an axis of symmetry not aligned along the principal crystal

directions, was observed in YBCO. The onset temperature of this signal was near  $T^*$  and size of the signal itself was larger in underdoped samples. Another study using much higher energy 1.5-eV light [5] demonstrated similar anisotropy, but with little temperature dependence in the linear response and a very prominent order parameter rise of the second-harmonic generation (SHG) signal at  $T^*$  that can be identified with inversion symmetry breaking. More recently, dc resistance anisotropy with axes of symmetry misaligned from the crystal axes of the copper oxygen planes was found in  $\text{La}_{2-x}\text{Sr}_x\text{CuO}_4$  [10]. A compilation of experiments on symmetry breaking in HTS cuprates can be found in Fig. 3 in Ref. [11]. The origin of these signals is unknown, but the data suggest the presence of a novel broken-symmetry phase, possibly nematic stripes [12] or bond currents [13,14]. The frequency dependence of these optical anisotropies may be crucial to resolving the microscopic origin of the broken symmetry. For example, since metals typically have a higher conductivity at lower frequencies, one may expect that metallic stripes could produce larger optical anisotropy as the probe frequency decreases.

In the present study we have measured polarization anisotropies for a number of HTS cuprate thin films grown on (100)  $\text{LaSrAlO}_4$  (LSAO) substrates over a broad frequency range. The energy range that we explore (1–2300 meV) spans most of the important energy scales in HTS cuprates, including the pair-breaking energy, the pseudogap energy, the plasma frequency, scattering rates, and the spin-gap energy. In our measurements, the real and imaginary components of

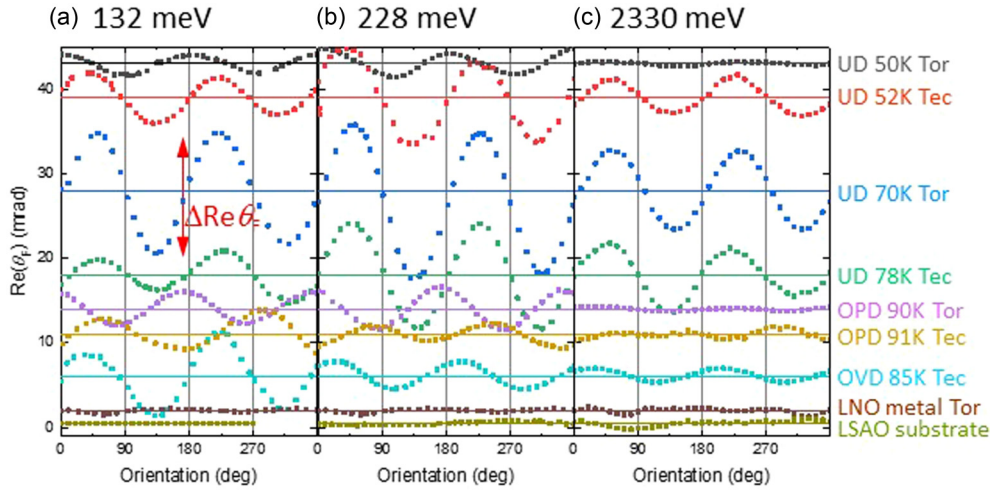


FIG. 1. Sample orientation dependence at 293 K of the Faraday angle at three energies: (a) 132 meV, (b) 228 meV, and (c) 2330 meV for YBCO films. Samples are listed with increasing doping towards the bottom of the figure. The films grown at Technion and Toronto are labeled Tec and Tor, respectively. The plots are offset vertically, with the zeros for each film given by the colored horizontal lines. The red double arrow indicates the peak-to-peak amplitude of the oscillations,  $\Delta\text{Re}\theta_F$ , which is used to quantify the LD signal.

the Faraday angle ( $\theta_F$ ) correspond to the polarization rotation and ellipticity, respectively, of the transmitted radiation. In the midinfrared range, linearly polarized, discrete spectral lines produced by  $\text{CO}_2$  (10.9–9.1  $\mu\text{m}$ , 114–135 meV) and CO (6–5.2  $\mu\text{m}$ , 205–237 meV) gas lasers are transmitted through the sample at near-normal incidence. Diode lasers covered the 500–2330-meV range. The change in the transmitted polarization is measured using photoelastic modulation techniques [15,16]. Broadband (100–600-meV) angle measurements are made at room temperature with a Bruker Vertex 70 Fourier transform infrared (FTIR) spectrometer using the same photoelastic modulation techniques. The THz measurements (2–6 meV) were made using THz time-domain spectroscopy [3,17].

The cuprate thin films used in this study were grown epitaxially on LSAO substrates using pulsed laser deposition (see Supplemental Material A and C for details [18–26]). LSAO substrates are well suited for these measurements since they are transparent in the THz/infrared/visible and are tetragonal, which eliminates any linear dichroism (LD) or linear birefringence signals from the substrate.

The complex Faraday angle at zero external magnetic field  $B$  was measured for YBCO,  $\text{La}_{1.85}\text{Sr}_{0.15}\text{CuO}_4$  (LSCO), and  $\text{LiNiO}_3$  (LNO) thin films grown on LSAO substrates as a function of incoming linear light polarization angle. Figure 1 shows the dependence of Faraday rotation [ $\text{Re}(\theta_F)$ ] on the YBCO sample orientation measured at 290 K for photon energies of (a) 132 meV, (b) 228 meV, and (c) 2330 meV. The panels are arranged with increasing doping towards the bottom of the figure. The samples are named according to whether they are underdoped (UD), optimally doped (OPD), or overdoped (OVD), followed by the superconducting critical temperature and where they were grown, namely Technion (Tec) or Toronto (Tor). The YBCO films grown in Toronto were 200 nm thick while the films grown at Technion were 100 nm thick, so the LD signals from the Technion films were multiplied by a factor of 2 to normalize all the signals to a 200-nm-thick film. All the HTS samples show clear LD response.

The response is sinusoidal as a function of the incident linear polarization with respect to the sample orientation and shows a  $180^\circ$  periodicity, which identifies the rotation as arising from linear polarization anisotropy, not circular polarization anisotropy. The UD 70 K Tor shows the largest peak-to-peak amplitude LD signal of 14 mrad at 228 meV. The LD signals in most of the HTS films, especially the UD samples, are maximized near 228 meV. Note that the relative phase of the LD oscillation with respect to the crystal axes is not the same for all the samples, e.g., OPD 90 K Tor and UD 50 K Tor start near nonzero values unlike the other films (see Supplemental Material D for details [18]). We also observe a frequency-dependent phase shift in some films, e.g., OVD 85 K Tec at 132 and 228 meV. There is no observable LD signal from the LSAO substrate nor from a metallic LNO film grown on LSAO, which makes us confident that the LD signal is intrinsic to the cuprate films (see Supplemental Material B [18]). The amplitude of the LD signal was obtained by a least-squares fit of the Faraday signal  $\frac{\Delta\text{Re}\theta_F}{2} \sin(2\phi + \varphi)$  to the sample orientation angle  $\phi$  and phase angle  $\varphi$ .

Figure 2 shows the energy dependence from 3 to 330 meV of  $\text{Re}(\theta_F)$  for YBCO films measured at 290 K and at 0 T. For all the underdoped samples, the LD signal increases as the probing energy increases from 100 meV towards 300–400 meV, then decreases towards 700 meV, and stays almost constant up to 2330 meV. There is a clear peak near 400 meV in the UD 70 K Tor sample. Similar behavior is observed in the UD 78 K Tec sample. These two samples were grown by different groups, which supports the reliability of these findings. UD 50 K Tor, UD 52 K Tec, and OPD 90 K Tor also show a peak in LD signal near 400 meV. The LD signals for optimally doped (OPD 91 K Tec) and overdoped (OVD 85 K Tec) films were much smaller and decreased with energy above 150 meV. Although OPD 91 K Tec and OVD 85 K Tec show similar frequency dependence, the LD signal for OVD 85 K Tec is over a factor of 2 larger than that of OPD 91 K Tec at 132 meV. On the other hand, the LD signal for the optimally doped sample OPD 90 K Tor is similar in magnitude

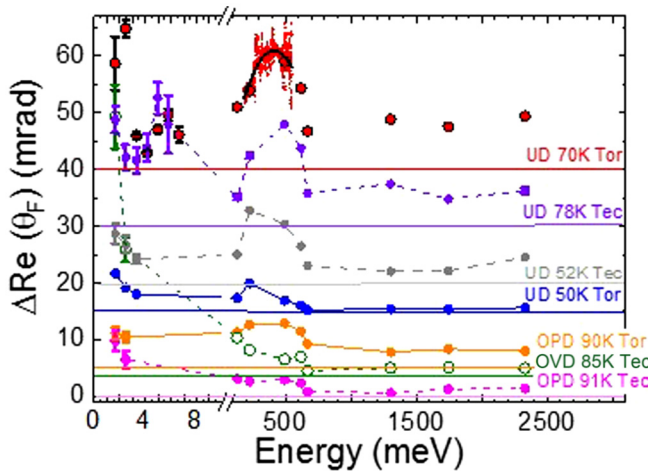


FIG. 2. Energy dependence of  $\Delta\text{Re}(\theta_F)$  for various YBCO films at 300 K. The symbols above 50 meV are from measurements using discrete laser emission lines. Symbols below 5 meV are from time-domain THz spectroscopy. The solid black line for UD 70 K Tor from 150 to 500 meV is a second-order polynomial fit to broadband FTIR measurements (small red dots). The dashed lines are guides to the eye to connect data from the same film. On data points where no error bars are shown, the error is smaller than the data symbol.

and energy dependence to the underdoped samples. The LD signal increases strongly in most samples as probe energy drops below 5 meV and there may be finite resonances in UD 70 K and UD 78 K near 2.5 and 5.0 meV, respectively. At the highest energy, 2330 meV, the LD signals for both optimally doped samples and the overdoped sample are nearly the same and well below the LD signals from the underdoped samples. In all the samples except for OPD 90 K Tor, the LD signal increases as the probe energy decreases below 5 meV. The increase in signal at low frequency is especially strong in OVD 85 K Tec.

The LD signal shown in Fig. 1 shows phase shifts [ $\varphi$  in the  $\text{Re}(\theta_F)$  fit] and small asymmetry in the lobe amplitudes. A lobe asymmetry in the LD oscillations can occur if the angle of incidence of the probing radiation is large ( $>10^\circ$ ). Therefore, great care was taken to make the angle of incidence smaller than  $5^\circ$ . If anisotropic conductivity, for example conducting “stripes,” is responsible for the LD signal, one may expect a phase-shift dependence on the angle of the stripes with respect to the Cu–O bonds. Note that we use the stripe analogy to help visualize the orientation of the anisotropy axis and do not claim that metallic stripes cause the LD signal. Figure 3 shows the LD signal measured at 132 meV and the orientation of conducting stripes that would be consistent with the measured signal in this scenario. Since the LSAO substrate is tetragonal, each edge of the substrate is parallel to one of the equivalent crystal axes of the film and we cannot distinguish one edge from the other. However, we can see in Fig. 3 that within such a scenario the stripes could be more parallel to an edge (UD 70 K Tor and LSCO) or closer to  $45^\circ$  from an edge (UD 50 K Tor and OPD 90 K Tor). Note that even within these two basic groups, small differences in the phase could be observed.

Figure 4(a) shows the temperature dependence of  $\text{Re}(\theta_F)$  at 132 meV when a sample is cooled at orientations of  $\pm 45^\circ$  with

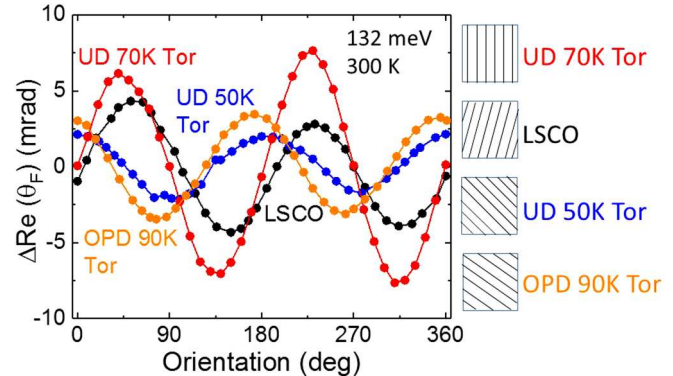


FIG. 3. LD signal at 293 K showing phase shifts and possible orientations of stripes that are consistent with these LD signals. The UD and OPD films are YBCO with indicated  $T_c$ s, whereas the LSCO film is optimally doped with a  $T_c$  of 34 K.

respect to the polarization of the incident light. The difference  $\Delta\text{Re}(\theta_F)$  between the curves increases as the sample is cooled, which indicates that the LD grows stronger at lower temperature. The LSAO substrate did not show any appreciable temperature dependence. Figure 4(b) tracks  $\Delta\text{Re}(\theta_F)$  as the samples cool from room temperature to 77 K. The underdoped samples show an increase in  $\Delta\text{Re}(\theta_F)$  with cooling while the optimally doped sample shows almost no temperature dependence. The overdoped sample behaves in a strikingly different way from the other films, including the optimally doped sample, with a relatively strong LD signal *decreasing* with cooling. In THz Faraday measurements [3], this same overdoped film showed a nonmonotonic temperature dependence, with two peaks and a dip below 100 K.

Our observations are consistent with the breaking of the naive mirror-plane symmetries of the  $\text{CuO}_2$  planes over a wide range of dopings. In this regard our results are consistent with previous THz spectroscopy measurements, although like the 1.5-eV reflectivity [4] and SHG [5] measurements we find that the symmetry breaking starts at temperatures well above the pseudogap temperature. In most samples, the LD signals are maximized in the few hundred meV energy range. The strongest LD signals tended to be found in mid-underdoped samples (see Supplemental Material D for details [18]). Although the samples are multidomain (twinned) and one would expect the contributions from crystal structure and the Cu–O chains from different domains to average out, the strong linear dichroism/birefringence signal suggests that the effect is macroscopic and persists across many domains over the large area ( $0.4\text{--}3\text{ mm}^2$ ) of the probing beam.

We now discuss possible origins of these effects. Both extrinsic and intrinsic origins must be considered. For the former it is important to note that the LD signal generally increases with decreased doping and it is important to note that if the signal has its origin in the greater conductivity of Cu–O chains, the trend would be opposite since underdoped samples have less metallic chains. The simplest explanation of the linear dichroism/birefringence structure found here could be in terms of one-dimensional (1D) conducting “stripe” or nematic structures, where conductivity is high along the wirelike stripes and low in the perpendicular direction. The

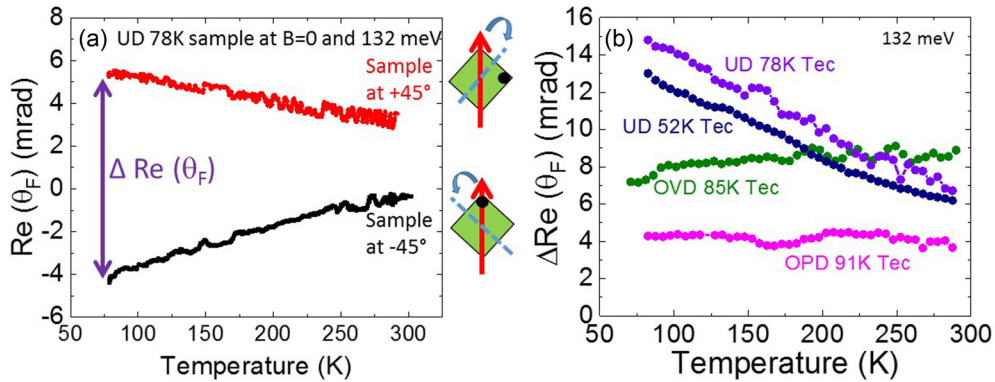


FIG. 4. (a) Temperature dependence of  $Re(\theta_F)$  at 132 meV in underdoped YBCO oriented at  $\pm 45^\circ$  with respect to the incident light polarization. (b) Temperature dependence of  $\Delta Re(\theta_F)$  for various dopings of YBCO at 132 meV.

observation [10] of anisotropy for in-plane dc transport measurements in LSCO is consistent with our observations. The authors in Ref. [10] suggest that the anisotropy is due to electronic nematicity that may not necessarily be aligned with the crystal axes. Among other aspects, these observations appear to rule out more conductive twin boundaries that can exist in YBCO as a source of the anisotropies as they do not exist in LSCO. However, although the previous terahertz polarimetry measurements on hole-doped  $YBa_2Cu_3O_y$  thin films reported the onset of a linear dichroic response near  $T^*$  that broke  $m_{ac}$  and  $m_{bc}$  symmetries [3], it was found later that not only were those symmetries already broken in the crystallographic structure of YBCO crystals above  $T^*$ , but that SHG experiments showed that the low symmetry of the pseudogap region could not be explained by stripe- or nematic-type orders alone [5,6].

As pointed out previously [3], another scenario that could account for the interesting tilted optical axes is gyrotrropic magnetoelectric birefringence. In such a magnetoelectric effect, magnetic order that breaks both time-reversal and inversion symmetries can cause linear birefringence where its zeros deviate from crystalline axes directions.  $Cr_2O_3$  is the most extensively investigated material with this physics [27]. In principle such an effect can account for a number of unique features of our data including the existence of the tilt. A model based on orbital currents predicts a magnetoelectric effect that can account for aspects of these data such as the tilt angle and a transition to another loop-current state that breaks mirror symmetry at lower temperature, resulting in a finite Kerr rotation [13]. Reference [14] predicts that tilted out-of-plane loop currents produce the same in-plane anisotropy, but also are consistent with the polar Kerr effect [4] and spin-polarized neutron scattering [28]. Recent SHG measurements [6] have found broken symmetries in the cuprates in the pseudogap and regions close to it that are consistent with an odd-parity magnetic order parameter that is broadly consistent with loop-current states.

The frequency dependence and maximum we find in the conductivity anisotropy near 300–400 meV may provide an important clue for resolving the microscopic mechanism responsible for the anisotropy. This finite-frequency maximum is not consistent with expectations for 1D conducting channels as the source of the anisotropy. Metallic response generally

peaks at zero frequency and one would expect anisotropic conductivity in wires to be maximum at zero frequency, where the dc conductivity is zero for electric fields applied perpendicular to the wires. One may envision scenarios in which there is a larger effective optical mass in one direction, but a larger scattering rate in the other that would give a conductivity anisotropy maximum at finite frequency, but this scenario seems unlikely. In contrast, a finite-frequency maximum is a reasonable expectation for magnetoelectricity as such effects are expected to vanish in the dc limit in a metal. It is important to point out that the frequency range of the maximum is roughly consistent with the frequency range of the midinfrared absorption [29] that has generally been associated with pseudogap physics. This energy is also close to the two-magnon frequency seen in Raman spectroscopy [30]. On the other hand, the LD signal in the THz increases strongly as frequency decreases from 6 to 1 meV, so there may be a metallic stripe component to the LD signal at lower frequency [3] or some other fluctuation mechanism is causing the enhancement of the LD signal at THz frequencies (e.g., Ref. [31]). The dc Hall angles measured by Ref. [10] in LSCO are similar in magnitude to our THz Faraday angles, so the upturn of the THz LD signal could be a shoulder of a zero-frequency peak rather than a finite-energy THz resonance. The general trend for higher LD as temperature decreases is consistent with higher conductivity, and therefore higher conductivity anisotropy for “wires,” as metals are cooled. This temperature dependence is also consistent with bringing the samples into the pseudogap phase as they are cooled down. The decrease in the LD signal for the OVD 85 K Tec sample as temperature decreases is extremely puzzling and may provide new clues to the symmetry-breaking mechanism(s). This sample also shows the most dramatic enhancement in the THz signal as the probe energy goes to zero. The nonmonotonic temperature dependence of the THz LD signal below 100 K [3] and the unusual temperature dependence that we observe for our overdoped sample in the infrared indicate that the LD temperature dependence is rich and could be critical to understanding the symmetry breaking that causes LD. This is a HTS cuprate that shows a decrease in the symmetry-breaking signal as the sample is cooled from room temperature.

In summary we have observed the temperature and doping dependence of polarization changes in the THz, infrared, and

visible range (3–2330 meV) with light incident on cuprate HTS. We find a twofold rotational symmetry in the Faraday rotation [ $\text{Re}(\theta_F)$ ] of the transmitted light and hence this signal is associated with linear dichroism. Such an effect occurs when electromagnetic radiation polarized along one direction is absorbed more strongly than radiation polarized in the perpendicular direction. Such polarization anisotropies can be generally associated with symmetry breakings and in this case the symmetries of the optical anisotropies are generally not directed along crystal axes showing the breaking of crystal mirror symmetries. The LD signal is broadly consistent with electronic nematicity that is not necessarily aligned with the crystal axes as well as a magnetoelectric effect. However, the signal shows a resonant behavior with a peak in the few hundred meV range, the presence of

which may argue against the polarization anisotropy coming from quasi-1D conducting channels and instead may be more consistent with magnetoelectric effects. The peak energy of 300–400 meV is an energy scale generally associated with the pseudogap.

We are indebted to D. Hsieh, S. A. Kivelson, C. M. Varma, and L. Zhao for helpful discussions. We gratefully acknowledge support from NSF-DMR Grant No. 1410599 (J.C.). A.G.M. and D.K.G. were supported by NSF Grant No. MCB 1616529 and DOE Grant No. DE-SC0016317. Work in Toronto was supported by NSERC, CFI-OIT, and the Canadian Institute for Advanced Research. J.Y.T.W. thanks Kejun Xu for laboratory assistance in Toronto. N.P.A. was supported by NSF Grant No. DMR 1905519.

---

[1] C. M. Varma, Non-fermi-liquid states and pairing instability of a general model of copper oxide metals, *Phys. Rev. B* **55**, 14554 (1997).

[2] M. E. Simon and C. M. Varma, Detection and Implications of a Time-Reversal Breaking State in Underdoped Cuprates, *Phys. Rev. Lett.* **89**, 247003 (2002).

[3] Y. Lubashevsky, L. Pan, T. Kirzhner, G. Koren, and N. P. Armitage, Optical Birefringence and Dichroism of Cuprate Superconductors in the THz Regime, *Phys. Rev. Lett.* **112**, 147001 (2014).

[4] J. Xia, E. Schemm, G. Deutscher, S. Kivelson, D. Bonn, W. Hardy, R. Liang, W. Siemons, G. Koster, M. Fejer, and A. Kapitulnik, Polar Kerr-Effect Measurements of the High-Temperature  $\text{YBa}_2\text{Cu}_3\text{O}_{6+x}$  Superconductor: Evidence for Broken Symmetry near the Pseudogap Temperature, *Phys. Rev. Lett.* **100**, 127002 (2008).

[5] L. Zhao, D. Torchinsky, J. Harter, A. D. L. Torre, and D. Hsieh, in *Encyclopedia of Modern Optics*, 2nd ed., edited by B. D. Guenther and D. G. Steel (Elsevier, Oxford, 2018), p. 207.

[6] L. Zhao, C. A. Belvin, R. Liang, D. A. Bonn, W. N. Hardy, N. P. Armitage, and D. Hsieh, A global inversion-symmetry-broken phase inside the pseudogap region of  $\text{YBa}_2\text{Cu}_3\text{O}_y$ , *Nat. Phys.* **13**, 250 (2017).

[7] B. I. Halperin, in *The Physics and Chemistry of Oxide Superconductors*, *Springer Proceedings in Physics* 60, edited by H. K. V. Lotsch (Springer-Verlag, Berlin, 1991), p. 439.

[8] N. P. Armitage, Constraints on Jones transmission matrices from time-reversal invariance and discrete spatial symmetries, *Phys. Rev. B* **90**, 035135 (2014).

[9] J. Orenstein, Optical Nonreciprocity in Magnetic Structures Related to High- $T_c$  Superconductors, *Phys. Rev. Lett.* **107**, 067002 (2011).

[10] J. Wu, A. Bollinger, X. He, and I. Božović, Spontaneous breaking of rotational symmetry in copper oxide superconductors, *Nature (London)* **547**, 432 (2017).

[11] J. Zhang, Z. Ding, C. Tan, K. Huang, O. O. Bernal, P.-C. Ho, G. D. Morris, A. D. Hillier, P. K. Biswas, S. P. Cottrell, H. Xiang, X. Yao, D. E. MacLaughlin, and L. Shu, Discovery of slow magnetic fluctuations and critical slowing down in the pseudogap phase of  $\text{YBa}_2\text{Cu}_3\text{O}_y$ , *Sci. Adv.* **4**, eaao5235 (2018).

[12] L. Nie, G. Tarjus, and S. A. Kivelson, Quenched disorder and vestigial nematicity in the pseudogap regime of the cuprates, *Proc. Natl. Acad. Sci. USA* **111**, 7980 (2014).

[13] C. M. Varma, Gyrotropic birefringence in the underdoped cuprates, *Europhys. Lett.* **106**, 27001 (2014).

[14] V. M. Yakovenko, Tilted loop currents in cuprate superconductors, *Physica B* **460**, 159 (2015).

[15] J. Cerne, M. Grayson, D. Schmadel, G. Jenkins, H. Drew, R. Hughes, A. Dabkowski, J. Preston, and P.-J. Kung, Infrared Hall Effect in High- $T_c$  Superconductors: Evidence for Non-Fermi-Liquid Hall Scattering, *Phys. Rev. Lett.* **84**, 3418 (2000).

[16] G. Acbas, M.-H. Kim, M. Cukr, V. Novák, M. A. Scarpulla, O. Dubon, T. Jungwirth, J. Sinova, and J. Cerne, Electronic Structure of Ferromagnetic Semiconductor  $\text{Ga}_{1-x}\text{Mn}_x\text{As}$  Probed by Subgap Magneto-optical Spectroscopy, *Phys. Rev. Lett.* **103**, 137201 (2009).

[17] D. K. George, A. V. Stier, C. T. Ellis, B. D. McCombe, J. Cerne, and A. G. Markelz, Terahertz magneto-optical polarization modulation spectroscopy, *J. Opt. Soc. Am. B* **29**, 1406 (2012).

[18] See Supplemental Material at <http://link.aps.org/supplemental/10.1103/PhysRevB.102.054520> for more information, which includes Refs. [19–26].

[19] H. Zhang, N. Gauquelin, C. McMahon, D. G. Hawthorn, G. A. Botton, and J. Y. T. Wei, Synthesis of high-oxidation  $\text{YBaCuO}$  phases in superoxygenated thin films, *Phys. Rev. Materials* **2**, 033803 (2018).

[20] I. Fridman, L. Gunawan, G. A. Botton, and J. Y. T. Wei, Scanning tunneling spectroscopy study of c-axis proximity effect in epitaxial bilayer manganite/cuprate thin films, *Phys. Rev. B* **84**, 104522 (2011).

[21] I. E. Trofimov, L. A. Johnson, K. V. Ramanujachary, S. Guha, M. G. Harrison, M. Greenblatt, M. Z. Cieplak, and P. Lindenfeld, Growth and properties of  $\text{La}_{2-x}\text{Sr}_x\text{CuO}_4$  films, *Appl. Phys. Lett.* **65**, 2481 (1994).

[22] G. Koren, A. Gupta, E. A. Geiss, A. Segmüller, and R. B. Laibowitz, Epitaxial films of  $\text{YBa}_2\text{Cu}_3\text{O}_{7-d}$  on  $\text{NdGaO}_3$ ,  $\text{LaGaO}_3$ , and  $\text{SrTiO}_3$  substrates deposited by laser ablation, *Appl. Phys. Lett.* **54**, 1054 (1989).

[23] M. K. Yakes, D. Gunlycke, J. L. Tedesco, P. M. Campbell, R. L. Myers-Ward, C. R. Eddy Jr., D. K. Gaskill, P. E. Sheehan,

and A. R. Laracuente, Conductance Anisotropy in Epitaxial Graphene Sheets Generated by Substrate Interactions, *Nano Lett.* **10**, 1559 (2010).

[24] A. Mukherjee, C. T. Ellis, M. M. Arik, P. Taheri, E. Oliverio, P. Fowler, J. G. Tischler, Y. Liu, E. R. Glaser, R. L. Myers-Ward, J. L. Tedesco, C. R. Eddy, D. K. Gaskell, H. Zeng, G. Wang, and J. Cerne, Giant magneto-optical Kerr enhancement from films on SiC due to the optical properties of the substrate, *Phys. Rev. B* **99**, 085440 (2019).

[25] J. Humlíček, R. Henn, and M. Cardona, Infrared vibrations in  $\text{LaSrGaO}_4$  and  $\text{LaSrAlO}_4$ , *Phys. Rev. B* **61**, 14554 (2000).

[26] R. Arpaia, E. Andersson, E. Trabaldo, T. Bauch, and F. Lombardi, Probing the phase diagram of cuprates with  $\text{YBa}_2\text{Cu}_3\text{O}_{7-\delta}$  thin films and nanowires, *Phys. Rev. Materials* **2**, 024804 (2018).

[27] R. V. Pisarev, B. B. Krichevskov, and V. V. Pavlov, Optical study of the antiferromagnetic-paramagnetic phase transition in chromium oxide  $\text{Cr}_2\text{O}_3$ , *Phase Transitions* **37**, 63 (1991).

[28] B. Fauqué, Y. Sidis, V. Hinkov, S. Pailhés, C. T. Lin, X. Chaud, and P. Bourges, Magnetic Order in the Pseudogap Phase of High- $T_C$  Superconductors, *Phys. Rev. Lett.* **96**, 197001 (2006).

[29] D. N. Basov and T. Timusk, Electrodynamics of high- $T_C$  superconductors, *Rev. Mod. Phys.* **77**, 721 (2005).

[30] G. Blumberg, P. Abbamonte, M. V. Klein, W. C. Lee, D. M. Ginsberg, L. L. Miller, and A. Zibold, Resonant two-magnon Raman scattering in cuprate antiferromagnetic insulators, *Phys. Rev. B* **53**, R11930(R) (1996).

[31] G. Koren and P. R. B. P. Lee, Observation of two distinct pairs fluctuation lifetimes and supercurrents in the pseudogap regime of cuprate junctions, *Phys. Rev. B* **94**, 174515 (2016).

*Correction:* The fourth sentence in the caption to Fig. 2 was improperly edited and has been fixed.